Photo Acoustic induced Ultrasound Imaging using F-K migration

Nitin Burman

A dissertation submitted for the partial fulfilment of BS-MS dual degree in Science

INDIAN INSTITUTE OF SCIENCE EDUCATION AND RESEARCH MOHALI

April 2019

Certificate of Examination

This is to certify that the dissertation titled "Photo Acoustic induced Ultrasound Imaging using the F-K migration" submitted by Mr. Nitin Burman (Reg. No. MS14073) for the partial fulfilment of BS-MS dual degree programme of the Institute, has been examined by the thesis committee duly appointed by the Institute. The committee finds the work done by the candidate satisfactory and recommends that the report be accepted.

Dr. Samir Kumar Biswas (supervisor)	Dr. Kamal P. Singh	Dr. Abhishek Chaudhuri

Date: April 2019

Declaration of Authorship

The work presented in this dissertation has been carried out by me under the guidance of Dr. Samir Kumar Biswas at the Indian Institute of Science Education and Research Mohali.

This work has not been submitted in part or in full for a degree, a diploma, or a fellowship to any other university or institute. Whenever contributions of others are involved, every effort is made to indicate this clearly, with due acknowledgement of collaborative research and discussions. This thesis is a bonafide record of original work done by me and all sources listed within have been detailed in the bibliography

Nitin Burman
(Candidate)

Date: April 2019

In my capacity as the supervisor of the candidates project work, I certify that the above statements by the candidate are true to the best of my knowledge.

Dr. Samir Kumar Biswas
(Supervisor)

Date: April 2019

"I think it is possible for ordinary people to choose to be extraordinary."

-Elon Musk

Acknowledgements

Firstly, I would like to thank my parents for guiding me on the right path and for all the support and positivity.

I would like to express my gratitude to Dr. Samir Kumar Biswas for letting me work on this research project and for opening my eyes to new stage of opportunity and strength.

Lastly, I would like to like to thank my special friends Riyaz, Jaideep and Tejasi for infusing confidence in me and with whom I can bounce my ideas around with.

List of Figures

Dedicated to my mom...

Contents

Abstract

Photoacoustic tomography(PAT) is emerging nowadays. It is offering a new perspective and opportunity in medical imaging. Due to its cost effective instrumentation, fast computation and better resolution, this particular area of the medical physics is growing rapidly. Recently, Dr. S.K. Biswas delineated the surface of the bone surface which was previously not possible using the PAT. He used the photo-acoustically induced ultrasound signal from the epidermis and recorded its reflection from the surface of the bone surface in the pulse echo mode. But, due to the inconsistency between the geometry of the detector array and shape of the reflector, the artefacts were produced in the reconstructed image as shown in his work.

In this thesis we have tried to solve this problem by using the Stolt's F-K migration. We test the proposed solution on the simulated signal and on the experimental data of finger like phantom.

Chapter 1

Introduction

Now-a-days various imaging modalities are developing which are not only getting computationally faster but also cost effective and more precise. One of the emerging imaging modality is the **Photoacoutic tomography**. It uses the **Photo-acoustic effect** exhibited by the **Photoacoustic material** finds out the image of source. It is offering a new perspective and opportunity in medical imaging. Due to its cost effective instrumentation, fast computation and better resolution, this particular area of the medical physics is growing very rapidly.

It has a potential of imaging blood flow in capillaries and veins[2]. When it is compared to the optical tomography, PAT can penetrate deeper, scatter less and hence produce the better resolution than the optical tomography[2]. Its non-ionizing radiation and better resolution puts it above the X-Ray tomography [2]. Its higher computation speed and cost effective instrumentation makes it advantageous than magnetic resonance imaging [2]. However if combined with the optical tomography we can get a improved contrast reconstructed image.

Photoacoustic effect is sensitive to light absorbing function tissues and proteins such as haemoglobin, melanin, etc, where at the counter side it is insensitive to non function tissue substances such as bone and similar type anatomical structure. Human organ consists of both functional and anatomical structure. Most of the PAT images show image of functional tissues such as haemoglobin, melanin, etc. whereas the anatomical structure for example, finger knee joint, which occupies almost 80% space is missing. However, in 2016 in Dr. SKB et. al "A Method for Delineation of Bone Surfaces in Photoacoustic Computed Tomography of the Finger" showed that bone can also be imaged. Since bone has a density of $1900 kg/m^3$ and is good reflector for ultrasound(US), the ultrasound produced by the PA material around the bone by the epidermis will be reflected by the bone and be recorded by the detectors. These signals are called **Photo acoustically generated Ultrasound (PAUS)**.

They can produce artefacts in PAT image reconstruction if not taken into account as show in figure 1.1. The blue line in figure 1.1(a) represents the $t1$ time taken by incoming waves to reach the detector D1 represents the incoming wave form the epidermis and red dotted line represents $t2 + t3$ time taken by the reflected wave to reach the detector. The distance from the time of flight from the signal is calculated as follow:

- For blue line: $x_1 = c \times t_1$
- For red line: $x_2 = c \times (t_2 + t_3)$

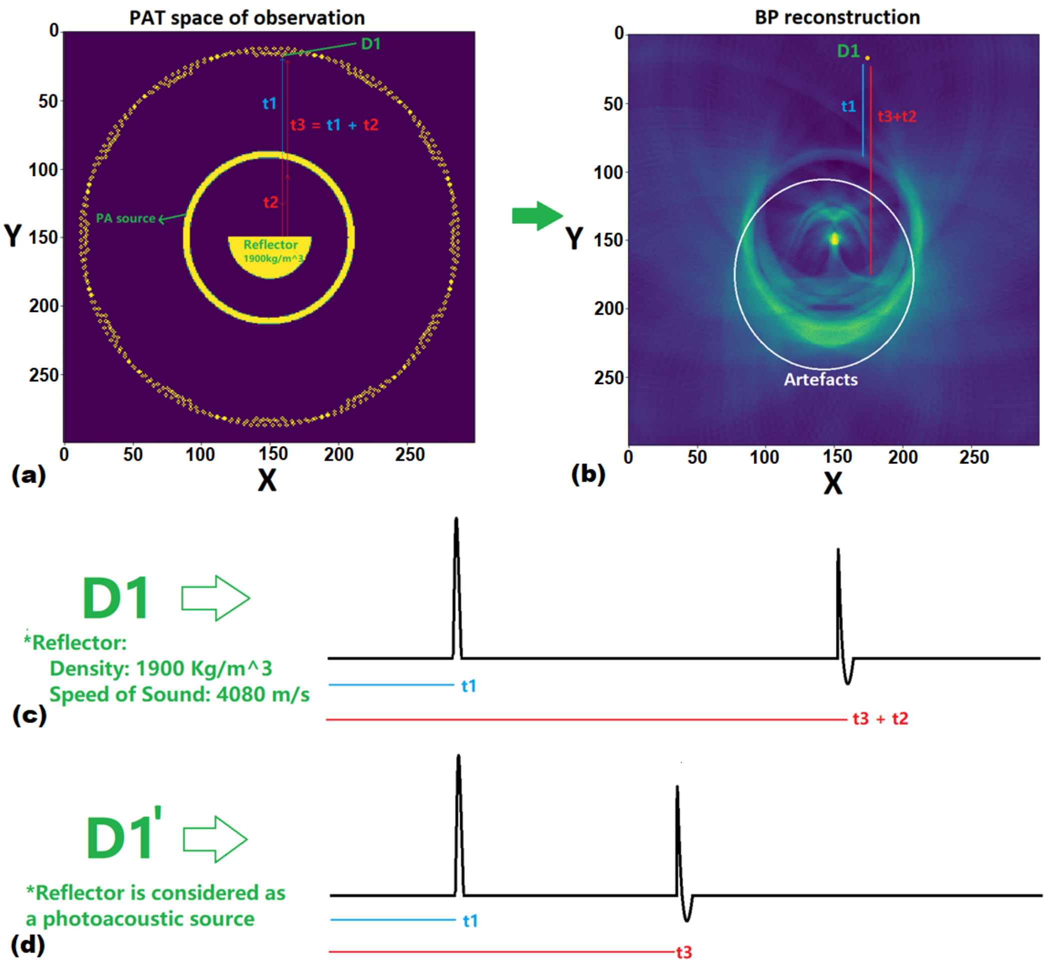

FIGURE 1.1: This figure is a simulation of the problem described in Dr. S.K Biswas et.al. "A new approach to depict bone surfaces in finger imaging in Photoacoustic tomography"[1]. Photoacoustic source is in the shape of ring and reflector has a density similar to bone i.e. $1900kg/m^3$. The density of the medium is same as of water i.e. $1000kg/m^3$

As seen in figure 1.1 (b), the x_1 distance corresponding to the time t_1 is plotted at its correct position but the reflected wave is plotted at x_2 distance corresponding to the time $t_2 + t_3$ which causes an artefact in the photoacoustic image. Similarly reflected signal from all other detector will cause the artefacts as shown in figure 1.1 (b).

To overcome this problem they have considered the epidermis(PA signal source) as the virtual US transmitter and photoacoustic probe as the detector array which captures the signal in the pulse echo mode as shown figure 1.2(a,c). They proposed two new algorithm **PAUS-I**, **PAUS-II**.

- **PAUS - I** : Single virtual ultrasound source is active at a time and the signal is recorded by all the 32 element of the detector array. Shown in figure 1.2(c)
- **PAUS - II** Single virtual ultrasound source is active at a time and the signal is recorded by a single detector which lie on the same line of the rotational center. Shown in figure 1.2(d)

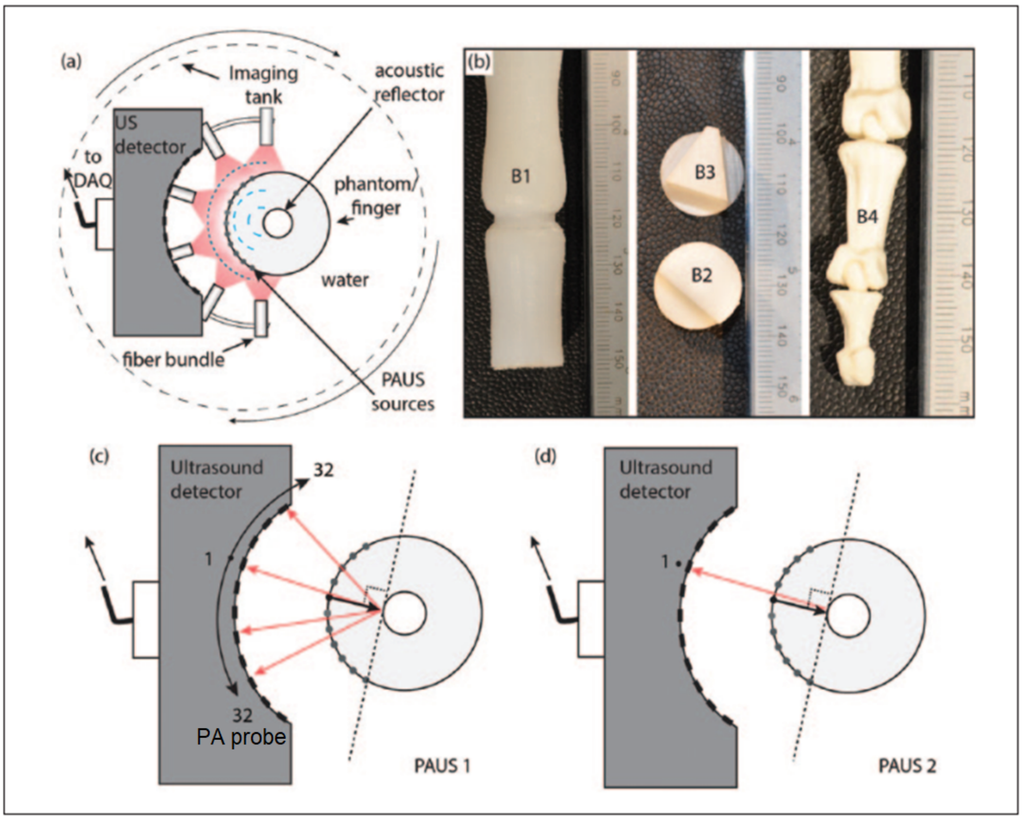

FIGURE 1.2: This figure was taken from Dr. S.K Biswas et.al. "A new approach to depict bone surfaces in finger imaging in Photoacoustic tomography"[1]. They developed two new algorithm, PAUS-I,II and tried to solve the reflection artefact problem. They have tested them on the phantom B1, B2, B3, B4 shown above.

They tested these algorithm on the different shapes of the phantom as shown in figure 1.2(b). The result of these new algorithms are shown in figure 1.3. Important thing to observe here is that reconstruction for the circular phantom(B1) is perfectly fine as shown in figure 1.3(a,d,g,j) . However we still see some artefacts in B2 and B3 phantom shapes as shown in figure 1.3(b,e,h,k,c,h,i,l). From this we concluded :

- Circular shape of reflector requires circular geometry of detector array.
- Linear shape of reflector requires linear geometry of detector array.

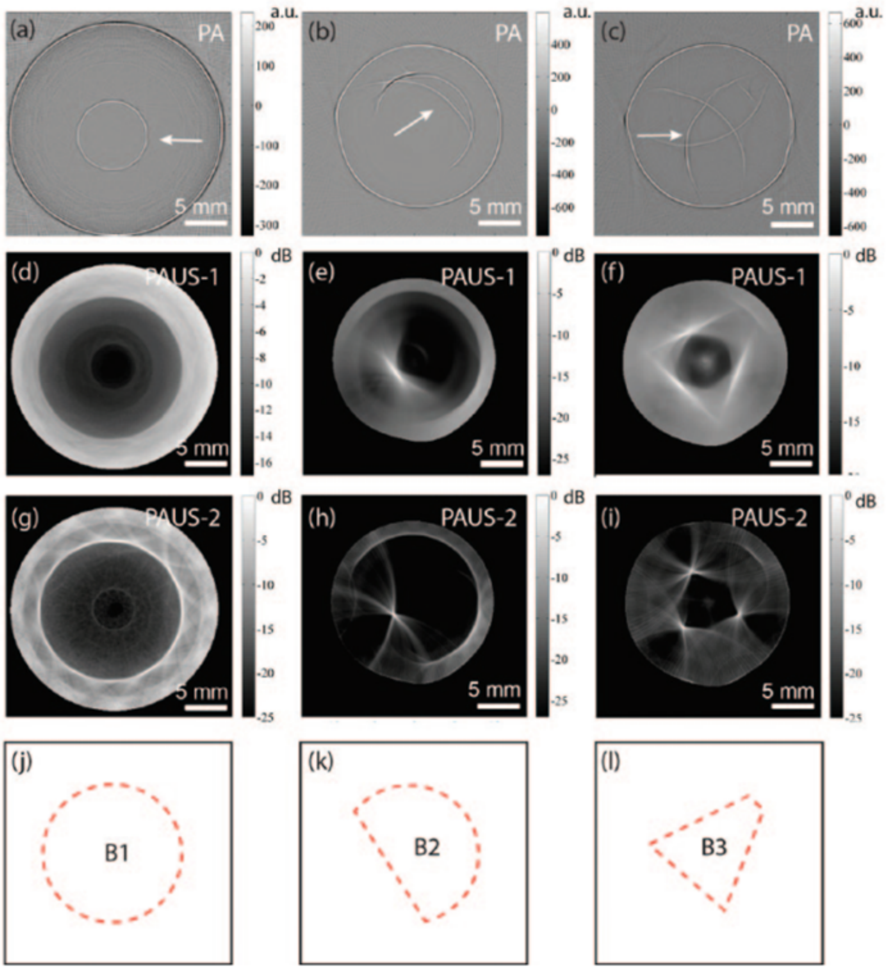

Figure 1.3: This figure was taken from Dr. S.K Biswas et.al. "A new approach to depict bone surfaces in finger imaging in Photoacoustic tomography"[1].It shows the result of PAUS I,II algorithms for different shapes phantom

The geometry of the detector array and the geometry of reflector should be similar when the conventional back-projection algorithms are used for reconstruction. The details of this fundamental problem is given in section 2.3.

We, in this thesis, show how to solve this fundamental problem by integrating the back-projection algorithm with the Stolt's F-K migration algorithm [3]. This algorithm is mainly used in the seismography(used in seismic imaging) to remove the artefact produced by the linear detector array and the shape of the reflector [3].

When the PA wave strikes on the surface of the reflector it get scattered which in result changes the resolution and the shape of the reflector surface. F-K migration takes that signal into the frequency domain and migrate back the frequencies to the time t=0 (the time at which the reflection happens). The theoretical details of F-K migration is given in section 2.4.

In Damien Garcia et. al, "Stolt's f-k migration for plane wave ultrasound imaging" [4] it is shown that the F-K migration can be implemented for the Plane Wave Imaging(PWI) which in our case restricts the geometry to the linear geometry of the detector array. In this thesis we will show how to implement the F-K migration on the circular geometry of detector array. We will show its implication on the experimental data produced by Dr. Samir Kumar Biswas in [1] paper and on the simulated data.

This thesis include the following things:

- Theoretical aspects necessary to understand and solve the described problem.
- Algorithm of the methods used.
- Integrated F-K migration algorithm.
- Results after the implication of our integrated F-K migration on experimental and simulated data.

Chapter 2

Theory

In this chapter we will talk about the mathematical details of the theoretical aspects necessary to understand and solve the described problem. We will also talk about the conventional back-projection algorithm and the F-K migration algorithm. We will also address the problem related with geometry of the detector array and the reflector surface in ultrasound tomography, and shape of the source in the photoacoustic tomography.

2.1 Photoacoustic effect

Basically, the PA effect can be described in the following steps:

1. Absorption of laser light* by tissue chromophore.
2. Conversion of this optical energy into the heat energy which leads to the rise in temperature.
3. Time varying thermoelastic expansion due to the temperature rise which leads to the formation of local pressure change which gives rise to the photoacoustic waves.

NOTE*: Nature of light must be pulsed and its duration must be around $10^{-9} sec$ which is less than the thermal and stress confinement of the object.

The partial differential equation for the photo-acoustic wave with a source as the pulsed laser can be described as:

$$\nabla^2 p(r,t) - \frac{1}{c^2}\frac{\partial^2 p(r,t)}{\partial^2 t} = -\frac{\beta}{C_p}\frac{\partial I(t)}{\partial t}A(r) \tag{2.1}$$

Where,

- $P(r,t)$: Pressure at r distance and t time
- $A(r)$: Absorbed optical energy density generated at r distance and at t time
- β: Isobaric volume expansion coefficient
- C_p: Isobaric specific heat of the medium
- $I(t)$: Time varying intensities of the laser light
- c: Acoustic speed

As mentioned above, if pulse duration of the laser is less than the stress confinement then $I(t)$ can be written as δt [5]

The solution to the equation (2.1) can be obtained by using the Green function's approach. Referring [5] for the detailed derivation

$$p(r,t) = \frac{\beta}{C_p}\frac{\partial}{\partial t}\left[\frac{1}{ct}\int_{R=ct} A(r')dr'\delta(t - \frac{|r'-r|}{c})\right] \tag{2.2}$$

Note: Photoacosutic effect is summarised in the flowchart given below in figure 2.1.

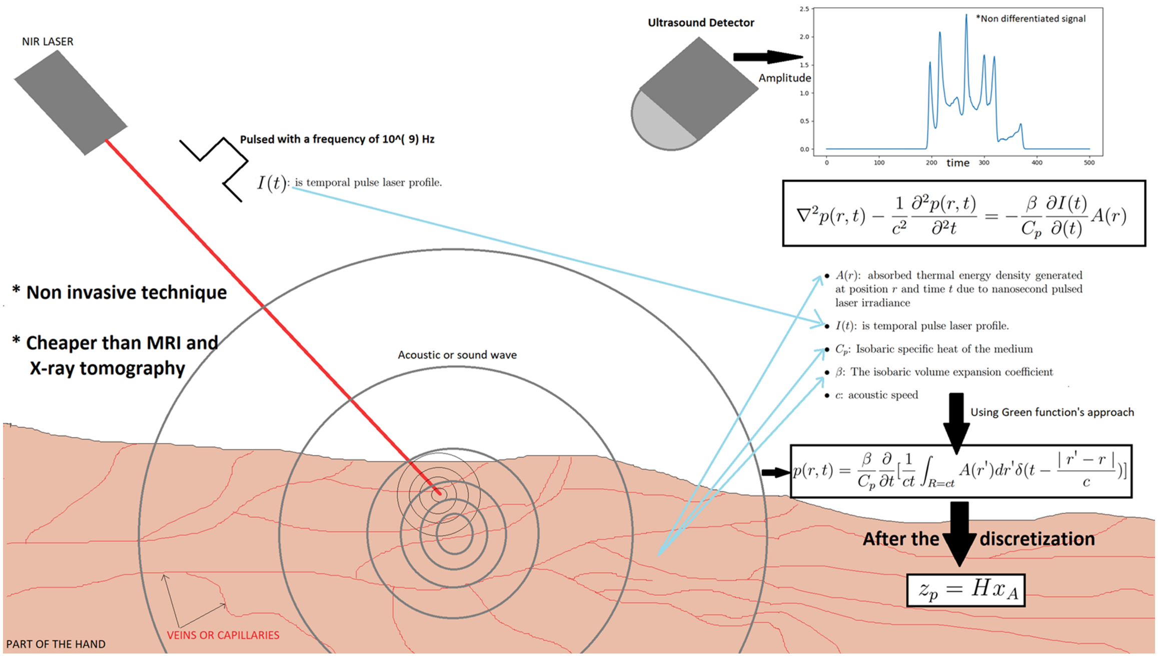

Figure 2.1: The Photo Acoustic Effect.

2.2 Photoacoustic tomography

Photoacoustic effect can be used to know the shape of the photoacoustic material in photo-acoustic tomography. It can produce higher resolution images as compared to the purely optical techniques, for example the Optical Coherence Tomography(OCT), Diffuse Optical Tomography. It is because we use near infrared laser light for the production of photoacoustic waves. It penetrates deeper and have lower scattering and attenuation than the white light used in the purely optical technique. The signal produced by the photoacoustic effect of the tissue choromophore is recorded by the ultrasound detectors. Various reconstruction algorithms are used to reconstruct the image of the source. Conventional way to reconstruct the source image is via the back projection algorithm.

Following are the steps to reconstruct the source image using the back projection algorithm in photoacoustic tomography.

1. Recording a signal by using the ultrasound detector as shown in figure 2.2(a)
2. Extracting the time of flight details from the signal as shown in as shown in figure 2.2(b)
3. Drawing a circle by taking a detector position as its center and its time of flight data as the radius(calculated using c = speed of sound) as shown in figure 2.2(c)
4. Repeating this for each detector as shown in figure 2.2(c).

Note: All these steps are summarised in the figure given below

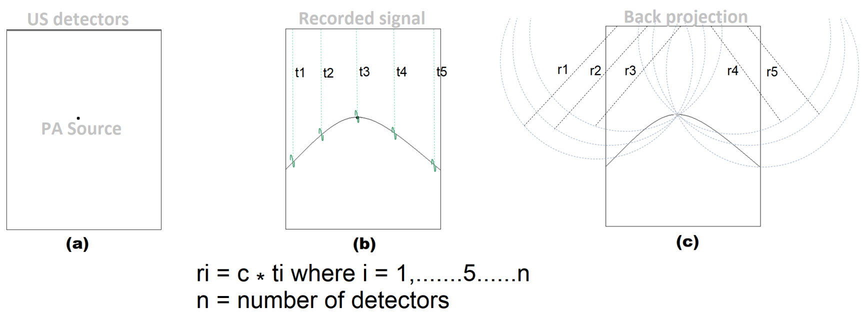

FIGURE 2.2: Backprojection algorithm is explained in this figure. (a) Space of observation, where the signal is recorded. (b) The recorded signal. (c) Reconstruction via backprojection

2.3 Geometry of detectors and the shape of the PA source

Geometry of detector array plays a big role when we are imaging in the tomography mode. Basically the geometry of detectors are chosen as per the idea of the shape of PA source . There can be two cases:

- Linear PA source
- Circular PA source

2.3.1 Linear PA source

When PAT is done with linear geometry of the detector array on the linear PA source, the signal and the reconstruction via backprojection looks like as shown in figure 2.3.

Important observation: The intersection of dotted circles in figure 2.3 will give the reconstructed image of PA source.

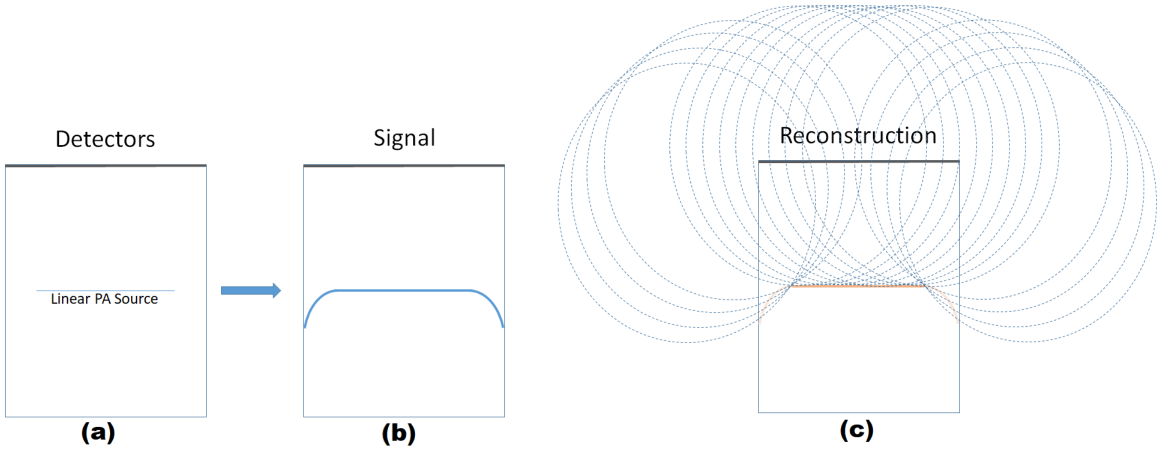

FIGURE 2.3: PAT with back projection for linear PA-source and linear detector array. The reconstruction is shown for the first peak each detector receive in their signal from the PA source.

When PAT is done with linear geometry of the detector array on the circular PA source, the signal and the reconstruction via backprojection looks like as shown in figure 2.4

Important Observation: In figure 2.4 the intersection of the dotted circles is creating artefacts in the reconstructed image. Those artefacts are denoted by the arrows in the figure.

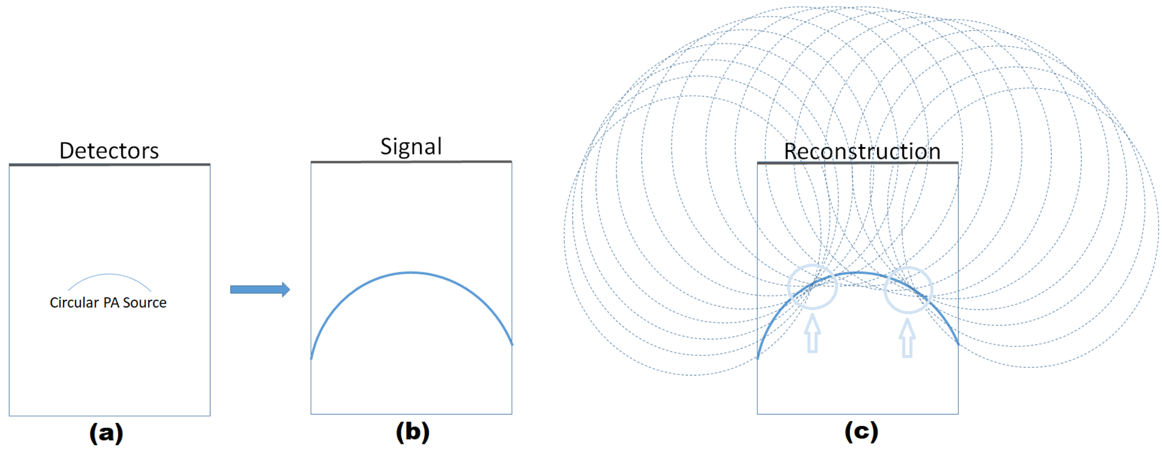

FIGURE 2.4: PAT with back projection with circular PA-source and linear detector array. In this figure the reconstruction is shown for the first peak each detector receive in their signal from the PA-source

2.3.2 Circular PA source

When PAT is done with the circular geometry of the detector array on the linear PA source, the signal and the reconstruction via backprojection looks like as shown in figure 2.5

Important observation: In figure 2.5, due to the more intersection of the dotted circle in the central region the linear PA source is not reconstructed properly.

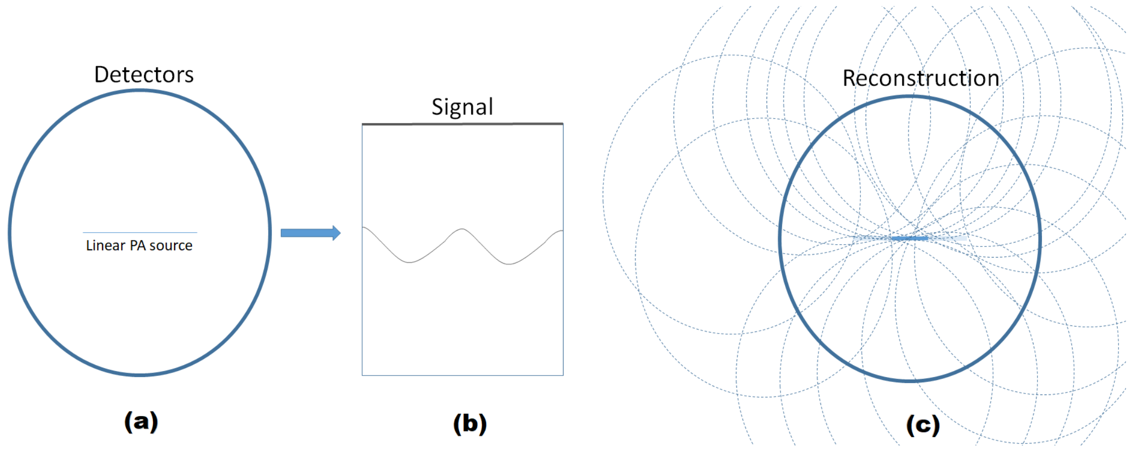

FIGURE 2.5: PAT with back projection with linear PA-source and circular detector array. In this figure the reconstruction is shown for the first peak each detector receive in their signal from the PA-source.

When PAT is done with the circular geometry of the detector array on the circular PA source, the signal and the reconstruction via backprojection looks like as shown in the figure 2.6.

Important observation: The intersection of the dotted circles in figure 2.6 will give the reconstructed image of the PA source

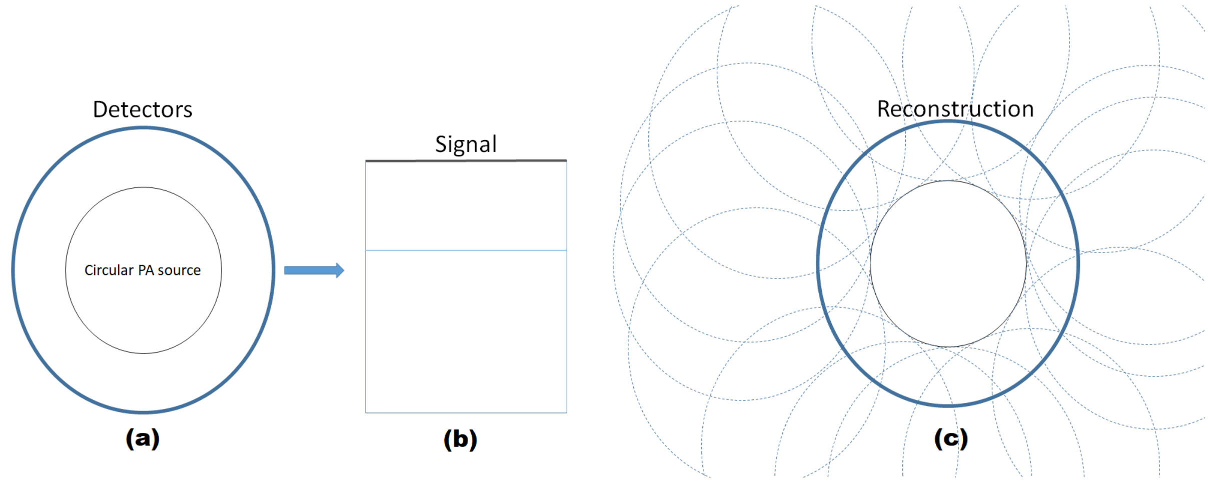

FIGURE 2.6: PAT with back projection with circular PA-source and circular detector array. In this figure the reconstruction is shown for the first peak each detector receive in their signal from the PA-source.

Note1: Backprojection reconstruction algorithm will remain same for the ultrasound tomography as explained in section 2.2. The only change will be that the ultrasound detector will change to ultrasound transducers and PA source will change to the reflector. Plane waves will go down towards the reflector from the transducers. After reflection the geometry of the waves will change according to the shape of reflector. The relation between the geometry of detector array and the shape of the reflector will be same for the ultrasound tomography as show above in section 2.3.1 and section 2.3.2.

Note2: In our problem, since our bone has **arbitrary shape**, using circular geometry of detector array is resulting in the formation of artefact while reconstructing the linear part as shown in figure 1.3(b,e,h,k). To solve this problem we developed an integrated F-K migration algorithm which is briefly explained in the following section.

2.4 F-K migration

F-K migration technique fixes the reflection artefacts and migrates back the signal to the time at which the waves just starts to emerge from the reflector (US tomography) and from the PA-source (PA tomography) i.e. at $t = 0$(see figure 2.7). Theoretical description of this algorithm is given below.

Lets assume that $\Psi(x,z,t)$ is the scalar wavefield that is a solution to

$$\nabla^2\Psi - \frac{1}{c}\frac{\partial^2}{\partial t^2}\Psi = 0 \tag{2.3}$$

We know the scaler wavefield at $z = 0$. We need to know the scalar wavefield at distance z at time $t = 0$ i.e. $\Psi(x,z,t=0)$ see figure 2.7

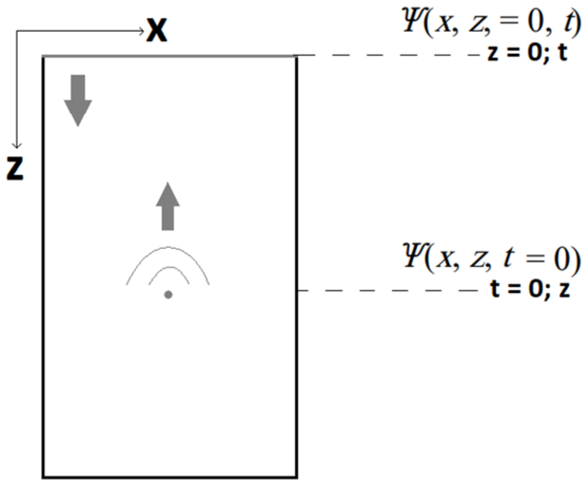

FIGURE 2.7: x-z plane, where linear transducer is placed on the x axis and reflector in x-z plane. The arrows represents the direction of propagation.

The Fourier transform of $\Psi(x,z,t)$ in the (k_x, f) spectrum is defined in the following way:

$$\Psi(x,z,t) = \iint_{-\infty}^{\infty} \phi(k_x, z, f) e^{2\pi\iota(k_x x - ft)} dk_x df \tag{2.4}$$

Now substituting equation (2.4) in equation (2.3) we get

$$\nabla^2\left[\iint_{-\infty}^{\infty} \phi(k_x, z, f) e^{2\pi\iota(k_x x - ft)} dk_x df\right] - \frac{1}{c}\frac{\partial^2}{\partial t^2}\left[\iint_{-\infty}^{\infty} \phi(k_x, z, f) e^{2\pi\iota(k_x x - ft)} dk_x df\right] = 0 \tag{2.5}$$

These derivatives can easily be taken inside the integral and can be evaluated to get

$$\iint_{-\infty}^{\infty}\left[\frac{\partial^2\phi(k_x,z,f)}{\partial z^2} + 4\pi^2\left[\frac{f}{c^2} - k_x^2\right]\phi(k_x,z,f)\right] e^{2\pi\iota(k_x - ft)} dk_x df = 0 \tag{2.6}$$

The left hand side of the equation (2.6) is the Fourier transform of the terms in the square bracket in the equation (2.6). Now since its right hand side is equal to zero, the function will also be equal to zero.

$$\frac{\partial^2}{\partial z^2}\phi(z) + 4\pi^2 k_z^2 \phi(z) = 0 \tag{2.7}$$

where,

$$k_z^2 = \frac{f^2}{v} - k_x^2 \tag{2.8}$$

Now we have formulated the problem in the (k_x, f) domain i.e. is a Fourier domain of (x, t). The boundary condition is now the Fourier transform of $\Psi(x, z = 0, t)$ over (x, t) i.e. $\phi(k_x, z = 0, f)$. Since, equation (2.7) is a second order differential equation, its unique general solution can be written as

$$\phi(k_x, z, f) = A(k_x, f)e^{2\pi\iota k_z z} + B(k_x, f)e^{-2\pi\iota k_z z} \tag{2.9}$$

where $A(k_x, f), B(k_x, f)$ are to be determined from the boundary condition. It is important to note that in (2.9) the two terms can be interpreted as the upgoing $(B(k_x, f)e^{-2\pi\iota k_z z})$ and downgoing$(A(k_x, f)e^{2\pi\iota k_z z})$ wavefield.

Since, we only have one boundary condition, i.e. $\phi(k_x, z = 0, f)$, in order to solve the problem we have to assume a limited model which assumes waves propagating in one direction only. This means that

$$A(k_x, f) = 0 \quad , \quad B(k_x, f) = \phi(k_x, z = 0, f) \tag{2.10}$$

Substituting (2.10) in (2.9) we get

$$\phi(k_x, z, f) = \phi(k_x, z = 0, f)e^{-2\pi\iota k_z z} \tag{2.11}$$

Substituting (2.10) solution in (2.4) we get

$$\Psi(x, z, t) = \iint_{-\infty}^{\infty} \phi(k_x, z = 0, f)e^{2\pi\iota(k_x x - k_z z - ft)} dk_x df \tag{2.12}$$

Now migrating (2.12) from time t to $t = 0$ we get our migrated solution

$$\Psi(x, z, t = 0) = \iint_{-\infty}^{\infty} \phi(k_x, z = 0, f)e^{2\pi\iota(k_x x - k_z z)} dk_x df \tag{2.13}$$

This solution has a disadvantage that it is inverse Fourier transform of function $\phi(k_z, z = 0, f)$. Stolt in 1978 suggested a change of variable from (k_x, f) to $(k_x, f(k_z))$ to make the migrated solution a inverse fourier transform of $\phi(k_x, z = 0, f(k_z))$. The variable change is defined by equation (2.8) which can be sovled for f

$$f = c \times \sqrt{k_x^2 + k_z^2} \tag{2.14}$$

$$\implies df = \frac{ck_z}{\sqrt{k_x^2 + k_z^2}} dk_z \tag{2.15}$$

Now substituting (2.14) and (2.15) in (2.13) we get

$$\Psi(x, z, t = 0) = \iint_{-\infty}^{\infty} \frac{ck_z}{\sqrt{k_x^2 + k_z^2}} \phi(k_x, z = 0, f(k_z)) e^{2\pi\iota(k_x x - k_z z)} dk_x dk_z \tag{2.16}$$

The equation (2.16) is now the final migrated signal which can simply be solved by using the FFT algorithm. The algorithm of the F-K migration can be described in the following steps:

Step 1: Recoding the signal $\implies \Psi(x, z = 0, t)$

Step 2: Taking the Fourier transform of the signal $\implies \phi(k_x, z = 0, f)$

Step 3: Changing the variable from f to $f(k_z)$ and rescaling the result with $\frac{ck_z}{\sqrt{k_x^2+k_z^2}} \implies \frac{ck_z}{\sqrt{k_x^2+k_z^2}} \times \phi(k_x, z = 0, f(k_z))$

Step 4: Taking the inverse Fourier transform of signal from step 3 to get the migrated solution back $\implies \Psi(x, z, t = 0) = \iint_{-\infty}^{\infty} \frac{ck_z}{\sqrt{k_x^2+k_z^2}} \phi(k_x, z = 0, f(k_z)) e^{2\pi\iota(k_x x - k_z z)} dk_x dk_z$

These points are summarised in the flow chart given below in the figure 2.8

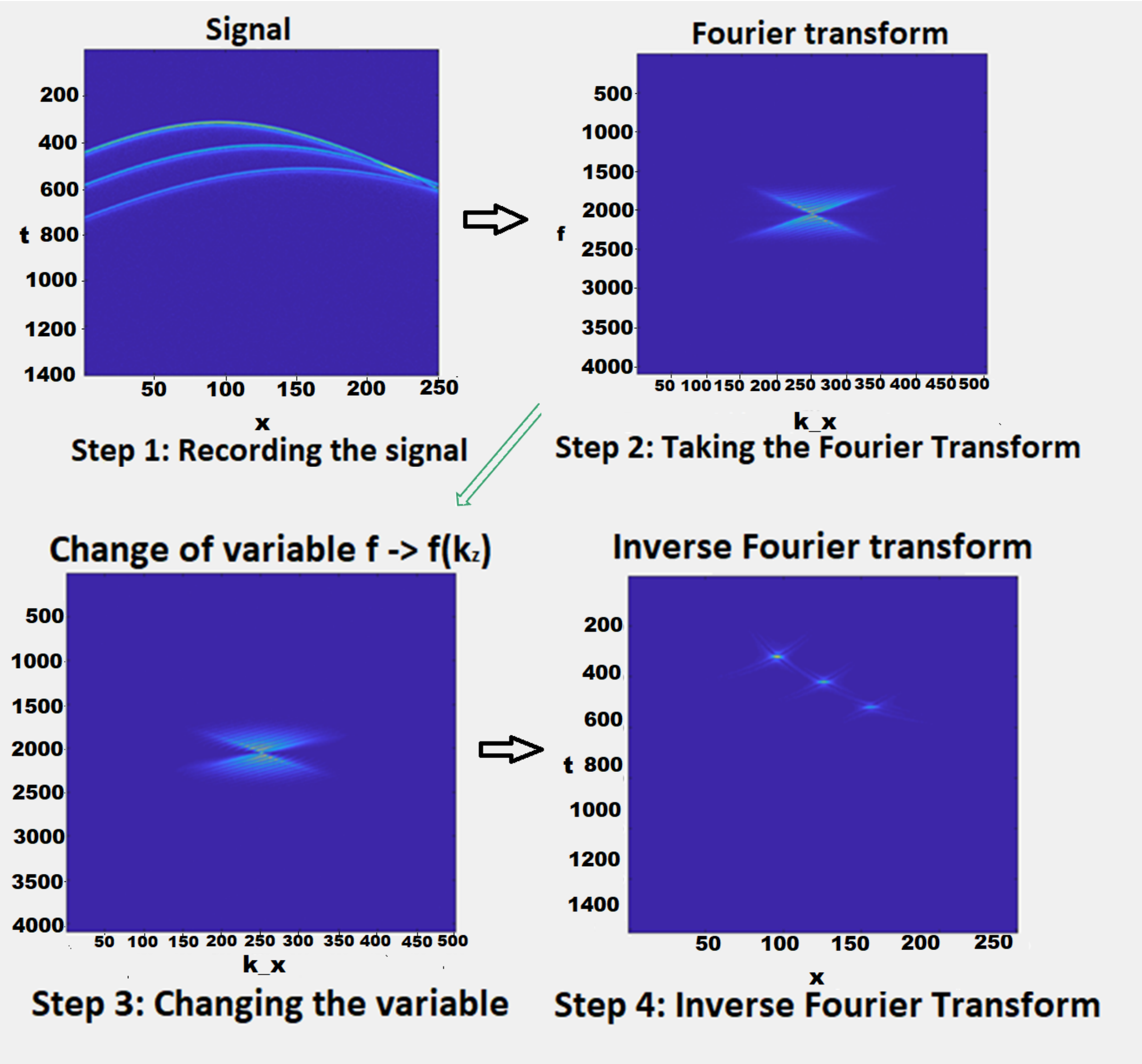

Figure 2.8: This figure represent the result of each step of the F-K migration algorithm.

Chapter 3

Implementation of the F-K migration

In previous chapter the F-K migration algorithm is derived for the plane waves. In this chapter we will show how to make use of the same F-K migration algorithm for the circular or any arbitrary shape of the wavefield. It basically includes 4 steps:

- Recording the signal
- Mapping signal onto a virtual detector array
- Implementing the F-K migration
- Remapping the signal onto the original detectors position

3.1 Step 0: Record the signal

The initial step is to record the signal using a circular detector array as shown in figure 3.1.

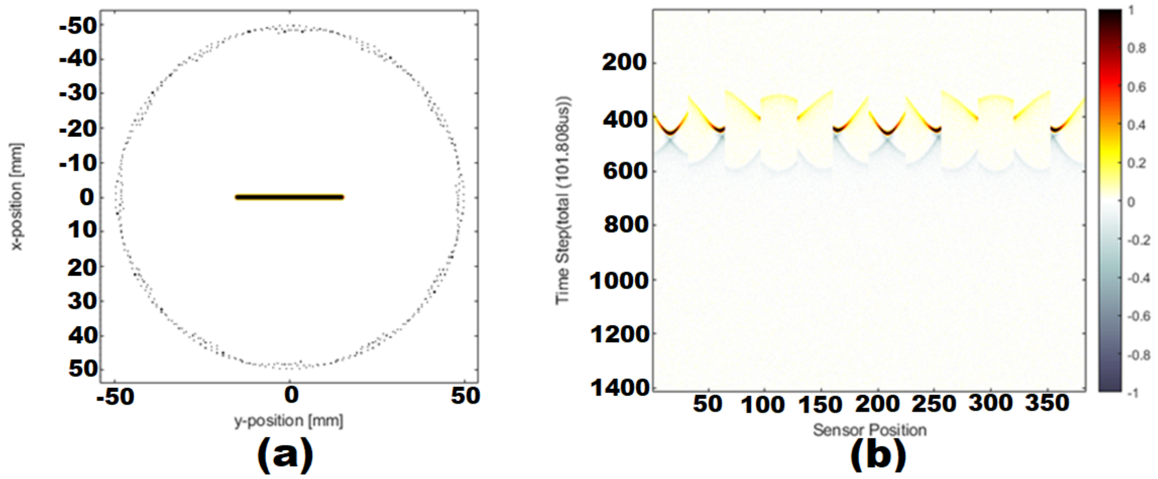

FIGURE 3.1: This figure shows the signal recorded by the detector of a linear PA source.

3.2 Step 1: Mapping signal onto a virtual linear detector array

After recording the signal, the next step is to map the signal onto the virtual linear detector array. This can be done by adding delay to signal from each detector. This delay is calculated from the mapping as shown in the figure 3.2.

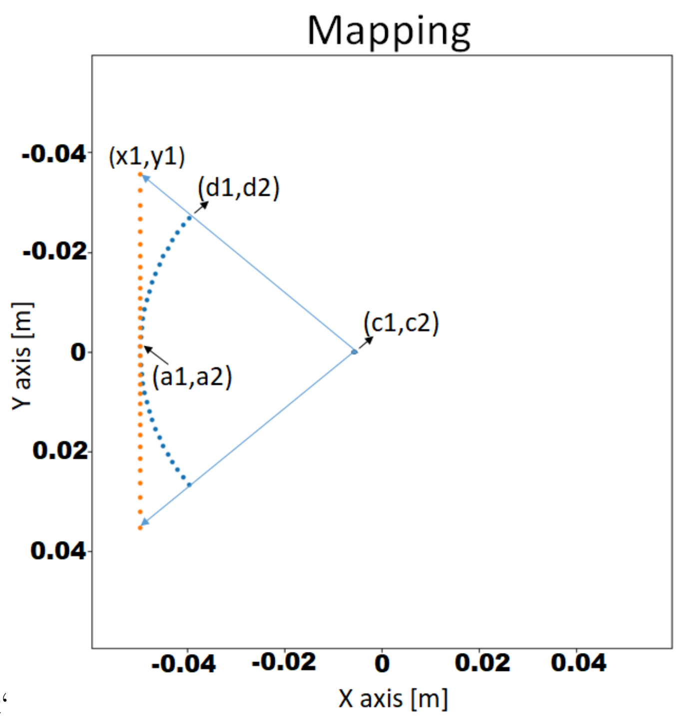

x‘

FIGURE 3.2: Mapping of the circular detector array to virtual linear detector array.

Lets assume $(c1, c2)$ be the center of the circular detector array. Let $(d1, d2)$ be the postion of the detector which is to be mapped. Let $(a1, a2)$ be the detector position of the middle detector as shown above in figure 3.2.

Intersection of the line passing through $(c1, c2)$, $(d1, d2)$ and the line $x = a1$ will give the coordinate of the mapped detector position i.e. $(x1, y1)$ as shown in figure 3.2.

$$\implies x1 = a1$$

$$\implies y1 = (a1 - c1)\left[\frac{d1 - c1}{d2 - c2}\right] + c2$$

Doing this for each detector position we get the mapped detector position as shown in figure 3.3

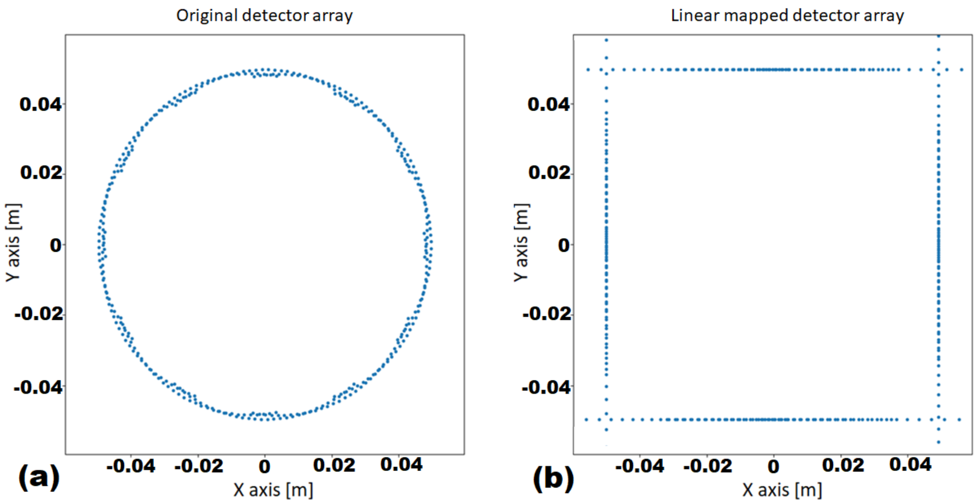

FIGURE 3.3: Mapping of the circular detector array to virtual linear detector array.

After calculating the mapped detector position, delay is calculated by finding the difference between the mapped and original detector position.

$$\implies t_{delay} = \frac{\sqrt{(x1 - d1)^2 + (y1 - d2)^2}}{c}$$

t_{delay} delay is added to the signal of the respective detector so that we can get a signal as if it was recorded from a linear detector. The signal after mapping will seem as if it was taken from a linear detector as shown in figure 3.4.

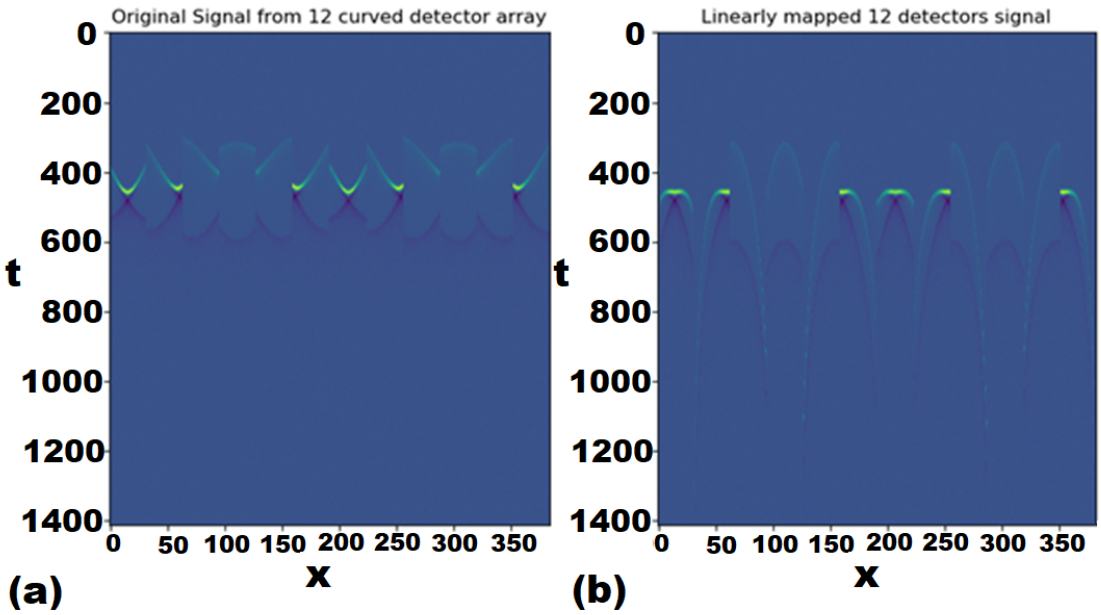

FIGURE 3.4: The figure on left represents the original data from the circular detector array and on the right hand side represents the linear mapped data.

3.3 Step 2: Implementing the F-K migration

After mapping the signal the F-K migration algorithm is implemented. The result after migration is shown in figure 3.5.

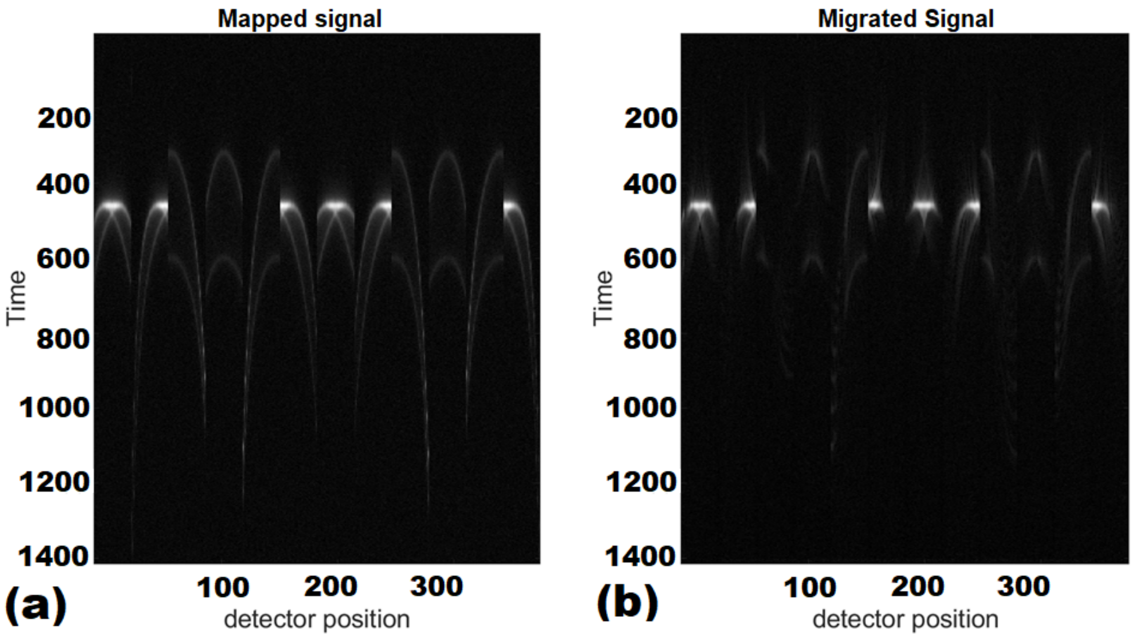

FIGURE 3.5: The figure on the left hand side represents the mapped data and on the right hand side represents the F-K migrated data.

3.4 Step 3: Remapping the signal onto the original detectors

After the implementation of F-K migration, the signal is remapped onto its original detector position. One can see the difference by comparing figure 3.4 and figure 3.6

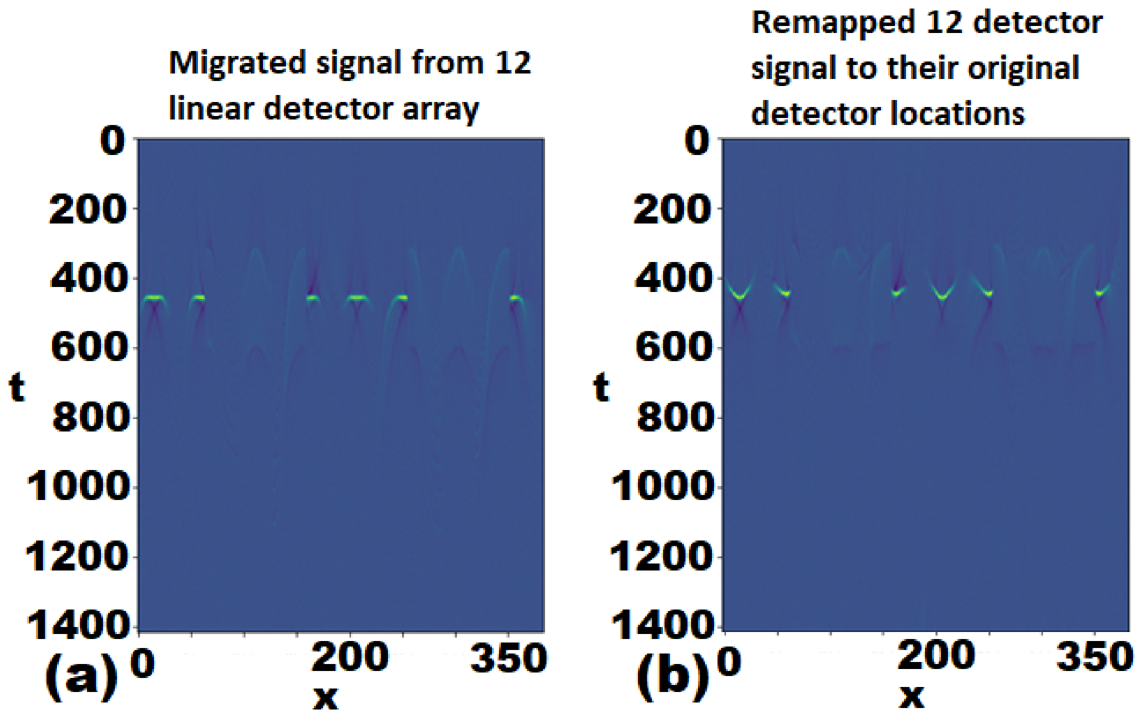

FIGURE 3.6: The figure on the left hand side represents the F-K migrated signal and on the right hand side represents remapped signal.

3.5 Step 4: Doing the dot projection

Now the final step is to do the reconstruction from the Linear mapped $\Longrightarrow$ F-Kmigrated $\Longrightarrow$ Remapped signal. In figure 3.7 the reconstruction using the dots is shown. F-K migration simply migrates back the signal to $t = 0$ which results in know in front of(perpendicularly down) which detector is our source.

In our case, since we are doing linear mapping $\Longrightarrow$ F-K migration $\Longrightarrow$ remapping, we need to do the reconstruction by plotting dots along the line of mechanical center of the circular detector array as show in figure 3.8. These dots will be plotted according to the time of flight calculated from the signal.

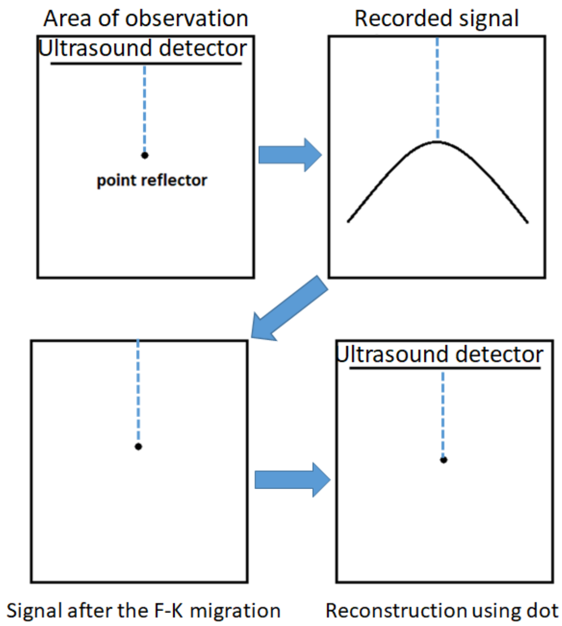

FIGURE 3.7: This figure represents the F-K migration and the backprojection via dots

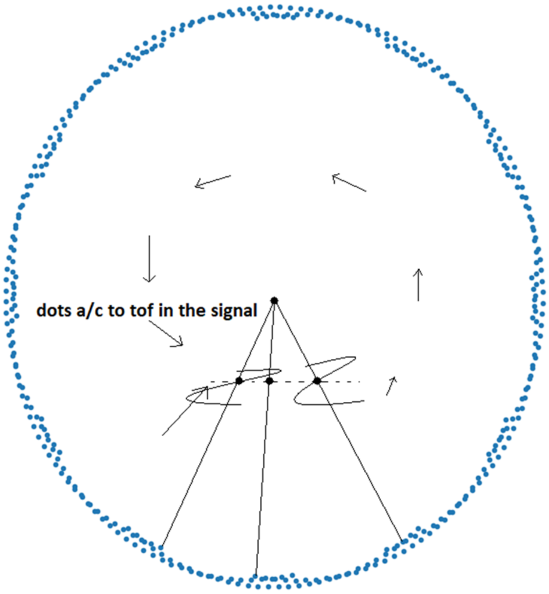

FIGURE 3.8: This figure represents the the backprojection via dots for the circular detector array

3.6 Conclusion

In this chapter, how to implement F-K migration on the the circular detector array is shown. The same methodology can be used to map and arbitrary shape of the detector to the virtual linear array of the detector. Python and MATLAB platform were used to do the Mapping, Remapping and F-K migration and Simulation respectively. In MATLAB, K-wave package was used to do the simulation of the photo-acoustic waves.

Similar simulation for ultrasound can also be done. For it, the methodology of doing the F-K migration will remain same. Only change will be that the ultrasound detector will become the ultrasound transducer and PA source will become the reflector.

This algorithm was tested on the PAUS simulation of the linear detector array data and on the experimental data recieved from Dr. S.K.Biswas. The results are shown in the next chapter.

Chapter 4

Results and Conclusion

In this chapter we will show the result after the implication of the F-K migration. The integrated F-K migration algorithm was tested on the simulated data and experimental data.

4.1 Simulated data

The simulation for photo-acoustically induced ultrasound(PAUS) waves was done in MATLAB using the k-wave package. For the simulation of PAUS waves **we kept the PA source at the location of the detector array** and recorded the signal from the curved surface of the reflector as shown in the figure 4.1.

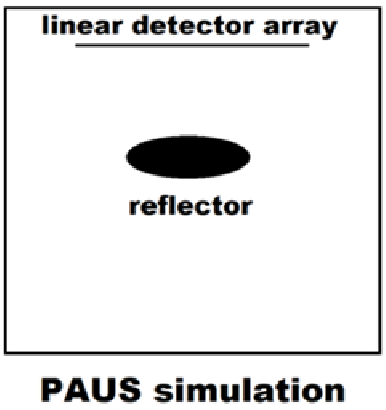

FIGURE 4.1: This figure represents the area of observation of the photoacoustically induced ultrasound simulation.

We get the result after the implementation of the F-K migration and the dot projection as shown in the previous chapter. The comparison of the backrprojection and the F-K migration $\Longrightarrow$ backprojection with dot of the simulation shown in figure 4.1 is shown in the figure 4.2

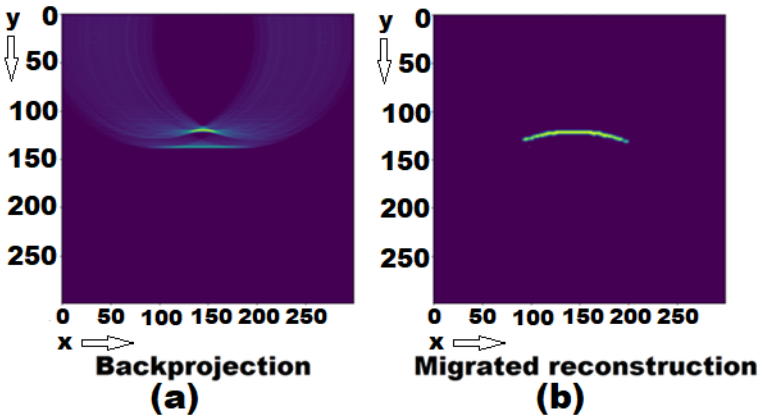

FIGURE 4.2: The figure on the left hand side the backprojection reconstruction and on the right hand side represents the F-K migration $\Longrightarrow$ backprojection with dots.

4.2 Experimental data

The data was provided to me by Dr. Samir Kumar Biswas. It is of a B2 phantom as described in figure 1.3(k) and its reconstruction is given in 1.3(h). We get the result after the implementation of the integrated F-K migration as told in previous chapter. The comparison of the backprojection and the implementation of the F-K migration is shown in figure 4.3

4.3 Conclusion

F-K migration was tested on linear array of detector and curved array of detectors. The backprojection algorithm completely fails to reconstruct the image of the curved reflector with linear array as shown in figure 4.2. But implementation of the F-K migration plus the backprojection with dots reconstructs the image back as shown in the migrated reconstructed section of the figure 4.2. However we could not get this result for the experimental data as seen in the figure 4.3. These are the following reasons why:

- We have used the linear interpolation when we change the variable f to $f(k_z)$ as shown in section 2.4. We have to use better interpolation methods to do the variable change, for example: cubic interpolation or sinc interpolation.

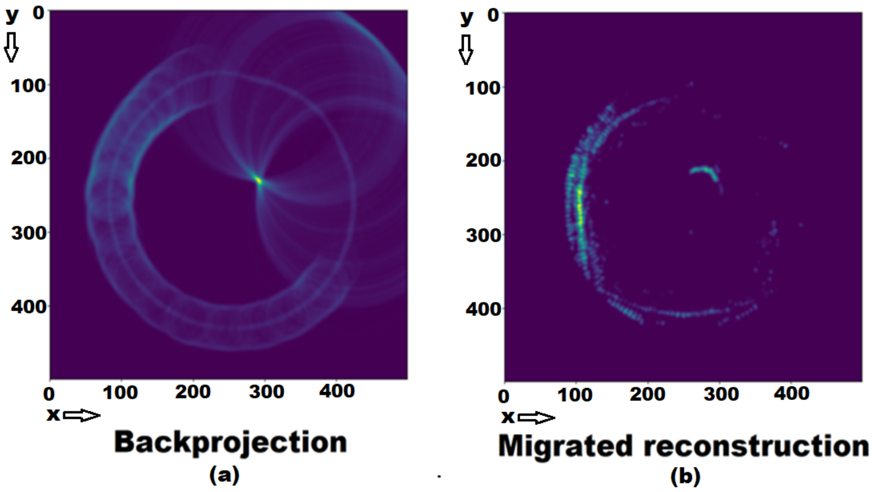

FIGURE 4.3: The figure on the left hand side the backprojection reconstruction and on the right hand side represents the integrated F-K migration

- When we are mapping the curved detector array onto a linear detector array as shown in figure 4.4 below, only the region A is properly mapped. So the signal which is coming from region B will not be properly mapped.
- Limitation of this integrated F-K migration algorithm is that the signal should come from the region A as shown in 4.4.

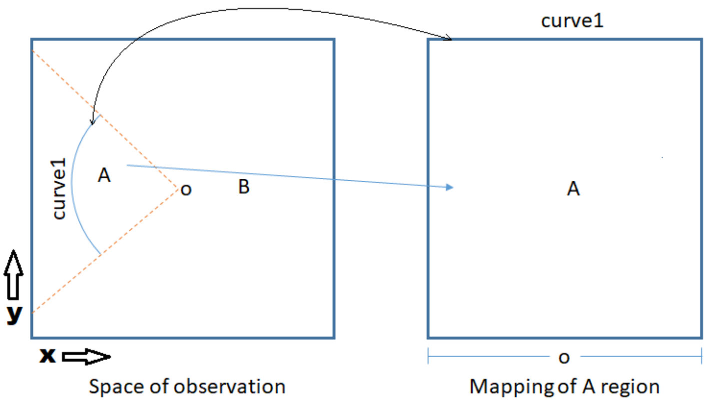

FIGURE 4.4: This figure represents the curve to linear mapping

Bibliography

[1] W.Steenbergen Dr. S.K. Biswas, P. vanEs and S. Manohar. A method for delineation of bone surfaces in photoacoustic computed tomography of the finger. *Ultrasonic Imaging*, pages 1–14, 2015.

[2] Junjie Yao Jun Xia and Lihong V. Wang. Photoacoustic tomography: principles and advances. *Electormagn Waves (Camb)*, pages 1–22, 2014.

[3] R.H. Stolt. Migration by fourier transform. *Geophysics*, pages 1–26, 1978.

[4] Stephan Muth Emmanuel Montagnon Jonathan Poree Damien Garcia, Louis Le Tarnec and Guy Cloutier. Stolt's f-k migration for plane wave ultrasound imaging. *IEEE Trans Ultrason Ferroelectr Freq Control*, 2014.

[5] W. Steenbergen R.M. Vasu S.K. Biswas, P. van Es and S. Manohar. Regularization free non-symmetric model matrix based iterative photoacoustic image reconstruction. *Un-published*.